IEEE Photonics Journal
An IEEE Photonics Society Publication

Open Access

Compensation for In-Phase/Quadrature Imbalance in Coherent-Receiver Front End for Optical Quadrature Amplitude Modulation

Volume 5, Number 2, April 2013

Md. Saifuddin Faruk
Kazuro Kikuchi, Fellow, IEEE

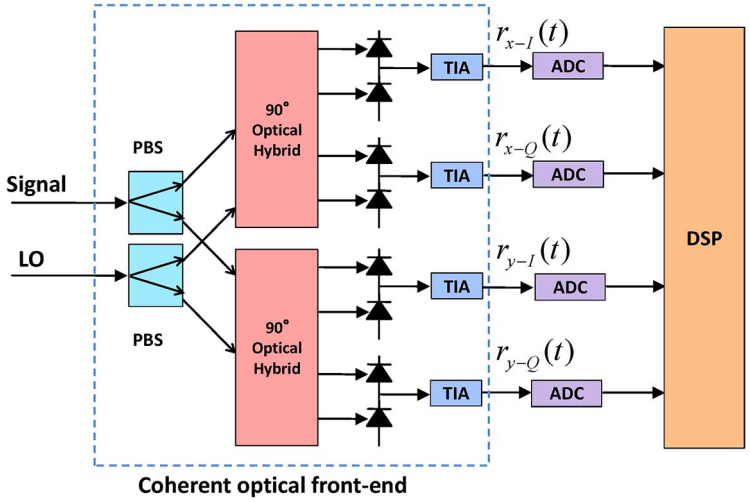

DOI: 10.1109/JPHOT.2013.2251872
1943-0655/$31.00 ©2013 IEEE

IEEE photonics SOCIETY

IEEE

Compensation for In-Phase/Quadrature Imbalance in Coherent-Receiver Front End for Optical Quadrature Amplitude Modulation

Md. Saifuddin Faruk[1] **and Kazuro Kikuchi,**[2] ***Fellow, IEEE***

[1]Department of Electrical and Electronic Engineering, Dhaka University of Engineering and Technology, Gazipur 1700, Bangladesh
[2]Department of Electrical Engineering and Information Systems, The University of Tokyo, Bunkyo-Ku, Tokyo 113-8656, Japan

DOI: 10.1109/JPHOT.2013.2251872
1943-0655/$31.00 ©2013 IEEE

Manuscript received January 11, 2013; revised February 26, 2013; accepted March 5, 2013. Date of publication March 13, 2013; date of current version March 22, 2013. Corresponding author: K. Kikuchi (e-mail: kikuchi@ginjo.t.u-tokyo.ac.jp).

Abstract: We propose a novel method of compensation for imbalance between in-phase (I) and quadrature (Q) channels in the front-end circuit of digital coherent optical receivers. Adaptive finite-impulse-response (FIR) filters in the butterfly configuration, which are commonly used for signal equalization and polarization demultiplexing, are modified so as to allow for adjustment of any imbalance between the IQ channels. IQ imbalances under consideration include the gain mismatch, the phase mismatch, and the timing-delay skew. Computer simulations for the dual-polarization quadrature-amplitude-modulation (QAM) format up to an order of 256 show that such IQ imbalances can severely degrade the system performance, especially for higher order QAM; however, using the proposed scheme, we can compensate for them without any significant penalty over a wide range of imbalances.

Index Terms: Coherent optical receivers, in-phase/quadrature imbalance, digital signal processing.

1. Introduction

The recent development of digital coherent optical receivers has brought the 100-Gbit/s dual-polarization quadrature phase-shift keying (QPSK) system into practical use [1]. For further increase in the bit rate of optical fiber transmission systems, quadrature amplitude modulation (QAM), where both of the in-phase (I) and quadrature (Q) components of an optical carrier are modulated in a multilevel manner, is the best candidate among various modulation formats [2]. However, when higher order QAM formats are employed, their performances are seriously impaired by imperfections of the systems, such as phase noise of the transmitter laser and the local oscillator [3], fiber nonlinearity [4], and imbalance between the IQ channels in the front end of coherent optical receivers [5]. In this paper, we focus on the impact of the imbalance between the IQ channels on QAM signals. We propose a novel IQ-imbalance compensation scheme, where the conventional adaptive finite-impulse-response (FIR) filters in the butterfly configuration are modified so as to allow for adjustment of any imbalance between the IQ channels.

The front end of coherent receivers employing phase and polarization diversities converts complex amplitudes of the incoming dual-polarization optical signal into the electrical domain by means of homodyne detection with a free-running local oscillator. It provides four outputs, namely, IQ

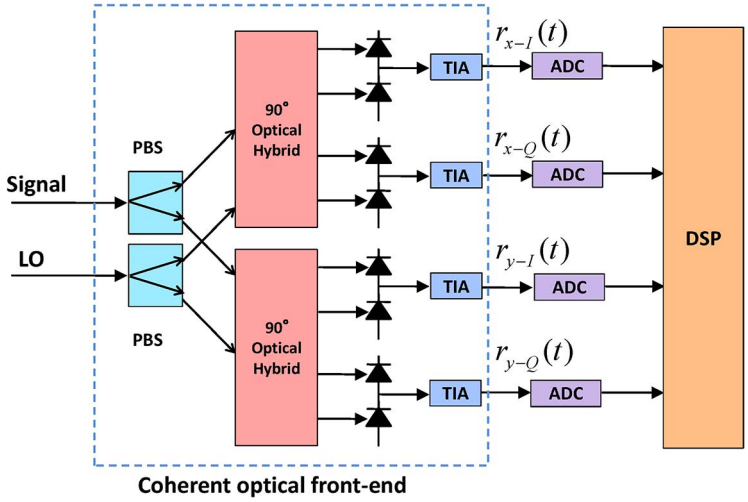

Fig. 1. Block diagram of the digital coherent receiver comprising phase and polarization diversities. LO: local oscillator, PBS: polarization-beam splitter, TIA: transimpedance amplifier, ADC: analog-to-digital converter, and DSP: digital signal-processing circuit.

components of the complex amplitudes for horizontal and vertical polarizations [6]. Fig. 1 shows the configuration of the front end composed of polarization-beam splitters (PBSs), 90° optical hybrids, balanced photodiodes, and transimpedance amplifiers (TIAs). The four outputs from TIAs are sent to analog-to-digital converters (ADCs) followed by a digital signal-processing (DSP) circuit.

Imperfection in any of the 90° optical hybrids, balanced photodiodes, and TIAs in the front end may introduce IQ imbalance stemming from the mismatch of the gain and/or the phase between the IQ ports [7]. In addition, timing mismatch between the IQ ports may also be induced by the difference in the physical path length of the circuit trace, which is known as the IQ delay skew [8]. These IQ imbalances degrade the system performance severely if they are left uncompensated in the DSP unit of the receiver.

Several methods of IQ-imbalance compensation in the digital domain have been reported so far [9]–[11]. In [9], the Gram–Schmidt orthogonalization procedure (GSOP) is investigated for the QPSK signal; however, when higher order QAM formats are employed, computational complexity is increased and very high ADC resolution is required. In [10], the compensation is done by the ellipse-correction method, which is neither applicable to higher order QAM signals nor effective when the optical signal-to-noise ratio (OSNR) is low. The IQ-imbalance equalizer based on the constant-modulus algorithm (CMA) is demonstrated for the QPSK signal in [11]; however, such an approach is again not applicable to higher order QAM signals. It should be also noted that none of the methods mentioned above can compensate for the IQ delay skew and that all of them need to use dedicated DSP circuits for IQ-imbalance compensation.

On the other hand, in this paper, we propose a novel scheme, which can overcome the difficulties of the previous schemes: First, our scheme can be applied to any modulation formats. Second, it can compensate for the IQ gain mismatch, IQ phase mismatch, and IQ delay skew all at once. Third, it can be implemented as a part of the conventional two-by-two butterfly-structured FIR filters, which have been commonly used for signal equalization and polarization demultiplexing.

In fact, our proposed scheme modifies the configuration of the conventional adaptive FIR filters in such a way that each of the complex-valued FIR filters is replaced with four real-valued FIR filters in an inner two-by-two butterfly structure. Then, our scheme has two input ports for each polarization, corresponding to the IQ outputs from the front end. Tap coefficients of the sixteen real-valued FIR filters can be updated using any stochastic-gradient-decent-based adaptation algorithm such as the decision-directed least-mean-square (DD-LMS) algorithm [12] and the CMA [13]. The initial convergence speed and the steady-state performance of the equalizer depend on the employed

adaptation algorithm. In this paper, we use the DD-LMS algorithm with the training mode. The training mode ensures fast and reliable initial convergence and then switched to the decision-directed mode. Such adaptation procedure provides the optimal steady-state performance for high-order QAM formats. By the proposed filter modifications, our scheme performs compensation for IQ gain/phase mismatch and IQ delay skew simultaneously, along with other conventional tasks of adaptive FIR filters such as sampling-phase adjustment [14], polarization demultiplexing [15], and compensation for polarization-mode dispersion (PMD) [16].

With intensive computer simulations using the 10-Gsymbol/s dual-polarization 4-, 16-, 64-, and 256-QAM formats, we find that the system performance severely degrades if we use the conventional FIR-filter structure in the presence of IQ imbalance; however, our scheme can fully compensate for IQ imbalance generated in the receiver front end over a wide range.

The organization of our paper is as follows: Section 2 presents the formulation of front-end IQ imbalance based on the transfer-function matrix. In Section 3, we propose the novel scheme for IQ-imbalance compensation together with the tap-adaptation algorithm. Section 4 deals with intensive computer simulations on higher order QAM signals, and we conclude our paper in Section 5.

2. Formulation of the Problem

Let $r_{x-I}(t)$ and $r_{x-Q}(t)$ respectively be received signals from the I and Q ports of the front-end circuit for the x-polarization component, when IQ imbalances are not present. Similarly, let $r_{y-I}(t)$ and $r_{y-Q}(t)$ be those for the y-polarization component. Then, the complex amplitude of the optical signal is reconstructed as

$$r_{x,y}(t) = r_{x-I,y-I}(t) + jr_{x-Q,y-Q}(t). \tag{1}$$

First, we consider the case that the IQ phase mismatch is included in the front end. In such a case, the I and Q axes in the complex plane are rotated by angles of δ_{x-I} and δ_{x-Q}, respectively, for the x-polarization component. Similarly, those angles for the y-polarization component are denoted as δ_{y-I} and δ_{y-Q}. IQ phase mismatches are given as $\delta_{x-I} - \delta_{x-Q}$ and $\delta_{y-I} - \delta_{y-Q}$ for x- and y-polarization components, respectively, which represent the offset from the correct angle of 90°. Using δ_{x-I}, δ_{x-Q}, δ_{y-I}, and δ_{y-Q}, the real and imaginary parts of the received complex amplitude $r^p_{x,y}(t)$ are expressed as

$$r^p_{x-I,y-I}(t) = \cos(\delta_{x-I,y-I})r_{x-I,y-I}(t) + \sin(\delta_{x-I,y-I})r_{x-Q,y-Q}(t) \tag{2}$$

$$r^p_{x-Q,y-Q}(t) = -\sin(\delta_{x-Q,y-Q})r_{x-I,y-I}(t) + \cos(\delta_{x-Q,y-Q})r_{x-Q,y-Q}(t). \tag{3}$$

When we define the transfer matrix $\mathbf{P}_{x,y}$ stemming from the IQ phase mismatch as

$$\mathbf{P}_{x,y} = \begin{bmatrix} \cos(\delta_{x-I,y-I}) & \sin(\delta_{x-I,y-I}) \\ -\sin(\delta_{x-Q,y-Q}) & \cos(\delta_{x-Q,y-Q}) \end{bmatrix} \tag{4}$$

equations (2) and (3) yield

$$\left[r^p_{x-I,y-I}(t), r^p_{x-Q,y-Q}(t)\right]^T = \mathbf{P}_{x,y}\left[r_{x-I,y-I}(t), r_{x-Q,y-Q}(t)\right]^T \tag{5}$$

which expresses the mutual coupling of real and imaginary parts of the complex amplitude.

Second, we consider the case that only the IQ gain mismatch is involved in the front end. In such a case, we can express the received complex amplitude as

$$r^g_{x,y}(t) = \alpha_{x-I,y-I}r_{x-I,y-I}(t) + j\alpha_{x-I,y-I}r_{x-Q,y-Q}(t). \tag{6}$$

In (6), α_{x-I} and α_{x-Q} are the gains of the I and Q ports, respectively, for the x-polarization component. Similarly, those values for the y-polarization component are α_{y-I} and α_{y-Q}. In case that $\alpha_{x-I} \neq \alpha_{x-Q}$, the IQ gain mismatch exists in the x-polarization port and it does in the y-polarization port when $\alpha_{y-I} \neq \alpha_{y-Q}$. The gain mismatching factor is defined as $\alpha_{x-I}/\alpha_{x-Q}$ and $\alpha_{x-I}/\alpha_{x-Q}$ for the

x- and y- polarization components, respectively. Equations (1) and (6) yield the transfer matrix for the IQ gain mismatch $\mathbf{G}_{x,y}$ as

$$\mathbf{G}_{x,y} = \begin{bmatrix} \alpha_{x-I,y-I} & 0 \\ 0 & \alpha_{x-Q,y-Q} \end{bmatrix} \tag{7}$$

which leads to

$$\left[r^g_{x-I,y-I}(t), r^g_{x-Q,y-Q}(t)\right]^T = \mathbf{G}_{x,y}\left[r_{x-I,y-I}(t), r_{x-Q,y-Q}(t)\right]^T. \tag{8}$$

Third, we consider the case that only the IQ delay skew is involved between the I and Q ports of the front end. When time delays in the four output ports of the front end are given as τ_{x-I}, τ_{x-Q}, τ_{y-I}, and τ_{y-Q}, the complex amplitude reconstructed from the front-end outputs can be expressed as

$$r^d_{x,y}(t) = r_{x-I,y-I}(t - \tau_{x-I,y-I}) + jr_{x-Q,y-Q}(t - \tau_{x-Q,y-Q}). \tag{9}$$

In case that $\tau_{x-I} \neq \tau_{x-Q}$, the IQ delay skew exists in the x-polarization component, whereas in case that $\tau_{y-I} \neq \tau_{y-Q}$, it does in the y-polarization component. We transform (9) into the frequency domain as

$$\left[R^d_{x-I,y-I}(\omega), R^d_{x-Q,y-Q}(\omega)\right]^T = \mathbf{D}_{x,y}(\omega)\left[R_{x-I,y-I}(\omega), R_{x-Q,y-Q}(\omega)\right]^T \tag{10}$$

where ω is the angular frequency of the optical signal measured from the carrier frequency; $R^d_{x-I,y-I}(\omega)$, $R^d_{x-Q,y-Q}(\omega)$, $R_{x-I,y-I}(\omega)$, and $R_{x-Q,y-Q}(\omega)$ are Fourier transforms of $r^d_{x-I,y-I}(t)$, $r^d_{x-I,y-I}(t)$, $r_{x-I,y-I}(t)$, and $r_{x-I,y-I}(t)$, respectively; and the transfer matrix $\mathbf{D}_{x,y}(\omega)$ is given as

$$\mathbf{D}_{x,y}(\omega) = \begin{bmatrix} \exp(j\omega\tau_{x-I,y-I}) & 0 \\ 0 & \exp(j\omega\tau_{x-Q,y-Q}) \end{bmatrix}. \tag{11}$$

On the other hand, frequency-domain expressions for $\mathbf{P}_{x,y}$ and $\mathbf{G}_{x,y}$ are the same as $\mathbf{P}_{x,y}$ and $\mathbf{G}_{x,y}$, since they are time independent. Therefore, the overall transfer function expressing the three kinds of IQ imbalances can be written in the frequency domain as

$$\mathbf{Q}_{x,y}(\omega) = \mathbf{P}_{x,y}\mathbf{G}_{x,y}\mathbf{D}_{x,y}(\omega). \tag{12}$$

Using (12), we find that the complex amplitude including the front-end IQ imbalances is measured as

$$\left[R^e_{x-I,y-I}(\omega), R^e_{x-Q,y-Q}(\omega)\right]^T = \mathbf{Q}_{x,y}(\omega)\left[R_{x-I,y-I}(\omega), R_{x-Q,y-Q}(\omega)\right]^T \tag{13}$$

in the frequency domain. To compensate for the IQ imbalances, we need to find the inverse matrix $\mathbf{Q}^{-1}_{x,y}(\omega)$, which eliminates the IQ phase mismatch, the IQ gain imbalance, and the IQ delay skew, as shown by

$$\left[R_{x-I,y-I}(\omega), R_{x-Q,y-Q}(\omega)\right]^T = \mathbf{Q}^{-1}_{x,y}(\omega)\left[R^e_{x-I,y-I}(\omega), R^e_{x-Q,y-Q}(\omega)\right]^T. \tag{14}$$

3. Proposed IQ Compensation Scheme

This section discusses how we can generate the inverse matrix $\mathbf{Q}^{-1}_{x,y}(\omega)$ using adaptive FIR filters. We assume that the linear transfer-function matrix of the link is given as $\mathbf{H}_f(\omega)$ in the absence of IQ imbalances. It is a two-by-two matrix including polarization-mode coupling. Fig. 2(a) shows the conventional adaptive FIR filters in the two-by-two butterfly structure. The discrete Fourier transform (DFT) of tap-coefficient vectors in Fig. 2(a) is defined as

$$\mathbf{h}_{ij}(n) = \left[h_{ij,0}(n), h_{ij,1}(n), \ldots, h_{ij,N}(n)\right]^T \tag{15}$$

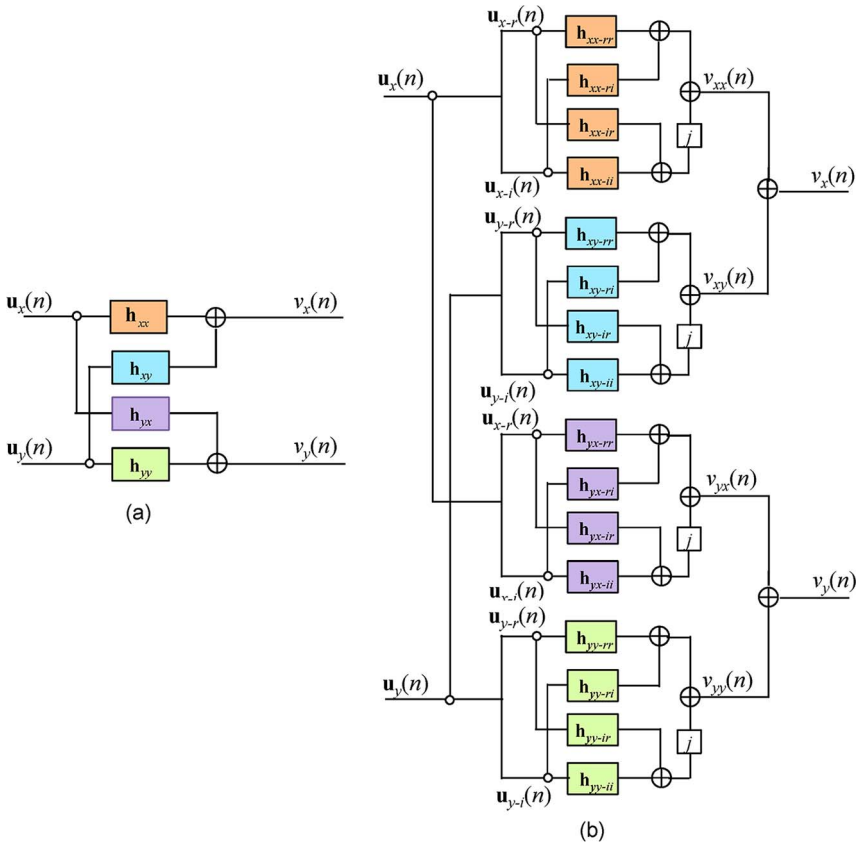

Fig. 2. Adaptive FIR-filter configurations used in digital coherent receivers. (a) Conventional configuration with four complex-valued FIR filters. (b) Our proposed configuration with sixteen real-valued FIR filters to enable IQ-imbalance compensation.

where $(i, j) = (x, y)$, n denotes the index of the data sequence, and N is the tap length. As discussed in [17], it can generate the inverse transfer function $\mathbf{H}_f^{-1}(\omega)$ in an adaptive manner. Since $\mathbf{H}_f^{-1}(\omega)$ is a two-by-two matrix with four complex elements, four butterfly-structured complex-valued FIR filters shown in Fig. 2(a) are capable of generating such matrix.

However, in order to compensate for IQ imbalances, tap-coefficient vectors $\mathbf{h}_{xx}(n)$ and $\mathbf{h}_{yx}(n)$ should generate $\mathbf{Q}_x^{-1}(\omega)$ because the input vector $\mathbf{u}_x(n)$ for them includes the IQ imbalances from the x-polarization channel. Similarly, $\mathbf{h}_{xy}(n)$ and $\mathbf{h}_{yy}(n)$ should generate $\mathbf{Q}_y^{-1}(\omega)$ to adjust the IQ imbalances of the y-polarization channel that is included in their common input vector $\mathbf{u}_y(n)$. Since $\mathbf{Q}_{x,y}^{-1}(\omega)$ is a two-by-two matrix that contains four independent elements, it is evident that the conventional FIR-filtering approach shown in Fig. 2(a) cannot generate $\mathbf{Q}_{x,y}^{-1}(\omega)$.

On the other hand, Fig. 2(b) shows the proposed configuration, where each complex-valued FIR filter is replaced by four real-valued FIR filters in an inner two-by-two butterfly structure. Our scheme works on two inputs corresponding to real and imaginary parts of the input complex amplitude. In the following, subscripts $(*)_r$ and $(*)_i$ correspond to the real and imaginary parts of a variable, respectively. With an optimum tap-adaptation algorithm, such a configuration ensures that

$$\mathrm{DFT}\begin{bmatrix} \mathbf{h}_{xx-rr}(n) & \mathbf{h}_{xx-ri}(n) \\ \mathbf{h}_{xx-ir}(n) & \mathbf{h}_{xx-ii}(n) \end{bmatrix} \simeq \mathbf{Q}_x^{-1}(\omega)\mathbf{H}_{11}(\omega) \tag{16}$$

$$\mathrm{DFT}\begin{bmatrix} \mathbf{h}_{xy-rr}(n) & \mathbf{h}_{xy-ri}(n) \\ \mathbf{h}_{xy-ir}(n) & \mathbf{h}_{xy-ii}(n) \end{bmatrix} \simeq \mathbf{Q}_y^{-1}(\omega)\mathbf{H}_{12}(\omega) \tag{17}$$

$$\mathrm{DFT}\begin{bmatrix} \mathbf{h}_{yx-rr}(n) & \mathbf{h}_{yx-ri}(n) \\ \mathbf{h}_{yx-ir}(n) & \mathbf{h}_{yx-ii}(n) \end{bmatrix} \simeq \mathbf{Q}_x^{-1}(\omega)\mathbf{H}_{21}(\omega) \tag{18}$$

$$\mathrm{DFT}\begin{bmatrix} \mathbf{h}_{yy-rr}(n) & \mathbf{h}_{yy-ri}(n) \\ \mathbf{h}_{yy-ir}(n) & \mathbf{h}_{yy-ii}(n) \end{bmatrix} \simeq \mathbf{Q}_y^{-1}(\omega)\mathbf{H}_{22}(\omega) \tag{19}$$

where four matrix elements of $\mathbf{H}_f^{-1}(\omega)$, i.e., $\mathbf{H}_{11}(\omega)$, $\mathbf{H}_{12}(\omega)$, $\mathbf{H}_{21}(\omega)$, and $\mathbf{H}_{22}(\omega)$, are transformed into two-by-two matrices $\mathbf{H}_{mn}(\omega)$ $((m,n)=(1,2))$ as

$$H_{mn}(\omega) \rightarrow \mathbf{H}_{mn}(\omega) = \begin{bmatrix} \mathrm{Re}(H_{mn}(\omega)) & -\mathrm{Im}(H_{mn}(\omega)) \\ \mathrm{Im}(H_{mn}(\omega)) & \mathrm{Re}(H_{mn}(\omega)) \end{bmatrix}. \tag{20}$$

Equation (20) is the transfer matrix for implementing a complex multiplication with well-known procedure of using four real multiplications. With such a modification, the matrix can be multiplied with a column vector consisting of the real and imaginary parts of the complex amplitude.

For the proposed configuration, four input column vectors are given by

$$\mathbf{u}_{(x,y)-(r,i)}(n) = \left[u_{(x,y)-(r,i)}(n), u_{(x,y)-(r,i)}(n-1), \ldots, u_{(x,y)-(r,i)}(n-N-1)\right]^T \tag{21}$$

and sixteen filter tap-coefficient vectors $\mathbf{h}_{pq-ab}(n)$, where $pq = xx, xy, yx$, or yy and $ab = rr, ri, ir$, or ii are written as

$$\mathbf{h}_{pq-ab}(n) = \left[h_{pq-ab}(n), h_{pq-ab}(n-1), \ldots, h_{pq-ab}(n-N-1)\right]^T. \tag{22}$$

The output signal $v_{pq}(n)$ is expressed as

$$v_{xx}(n) = \mathbf{h}_{xx-rr}(n)\mathbf{u}_{x-r}(n) + \mathbf{h}_{xx-ri}(n)\mathbf{u}_{x-i}(n) + j\{\mathbf{h}_{xx-ir}(n)\mathbf{u}_{x-r}(n) + \mathbf{h}_{xx-ii}(n)\mathbf{u}_{x-i}(n)\} \tag{23}$$

$$v_{xy}(n) = \mathbf{h}_{xy-rr}(n)\mathbf{u}_{y-r}(n) + \mathbf{h}_{xy-ri}(n)\mathbf{u}_{y-i}(n) + j\{\mathbf{h}_{xy-ir}(n)\mathbf{u}_{y-r}(n) + \mathbf{h}_{xy-ii}(n)\mathbf{u}_{y-i}(n)\} \tag{24}$$

$$v_{yx}(n) = \mathbf{h}_{yx-rr}(n)\mathbf{u}_{x-r}(n) + \mathbf{h}_{yx-ri}(n)\mathbf{u}_{x-i}(n) + j\{\mathbf{h}_{yx-ir}(n)\mathbf{u}_{x-r}(n) + \mathbf{h}_{yx-ii}(n)\mathbf{u}_{x-i}(n)\} \tag{25}$$

$$v_{yy}(n) = \mathbf{h}_{yy-rr}(n)\mathbf{u}_{y-r}(n) + \mathbf{h}_{yy-ri}(n)\mathbf{u}_{y-i}(n) + j\{\mathbf{h}_{yy-ir}(n)\mathbf{u}_{y-r}(n) + \mathbf{h}_{yy-ii}(n)\mathbf{u}_{y-i}(n)\}. \tag{26}$$

Then, the final outputs from the FIR-filter configuration, i.e., $v_x(n)$ and $v_y(n)$, are computed as

$$v_x(n) = v_{xx}(n) + v_{xy}(n) \tag{27}$$

$$v_y(n) = v_{yx}(n) + v_{yy}(n). \tag{28}$$

The error signal for updating the tap coefficients using the DD-LMS algorithm is calculated as

$$e_{x,y}(n) = d_{x,y}(n) - v_{x,y}(n) \tag{29}$$

where $d_{x,y}(n)$ is either the training symbol in the training mode or the symbol decoded from $v_{x,y}(n)$ in the tracking mode.

Finally, based on the DD-LMS algorithm, the filter tap coefficients are updated as

$$\mathbf{h}_{pq-rr}(n+1) = \mathbf{h}_{pq-rr}(n) + \mu e_{p-r}(n)\mathbf{u}_{q-r}(n) \tag{30}$$

$$\mathbf{h}_{pq-ri}(n+1) = \mathbf{h}_{pq-ri}(n) + \mu e_{p-r}(n)\mathbf{u}_{q-i}(n) \tag{31}$$

$$\mathbf{h}_{pq-ir}(n+1) = \mathbf{h}_{pq-ir}(n) + \mu e_{p-i}(n)\mathbf{u}_{q-r}(n) \tag{32}$$

$$\mathbf{h}_{pq-ii}(n+1) = \mathbf{h}_{pq-ii}(n) + \mu e_{p-i}(n)\mathbf{u}_{q-i}(n) \tag{33}$$

where μ is the step-size parameter, and $e_{x-r,y-r}(n)$ and $e_{x-i,y-i}(n)$ are the real and imaginary parts of $e_{x,y}(n)$, respectively.

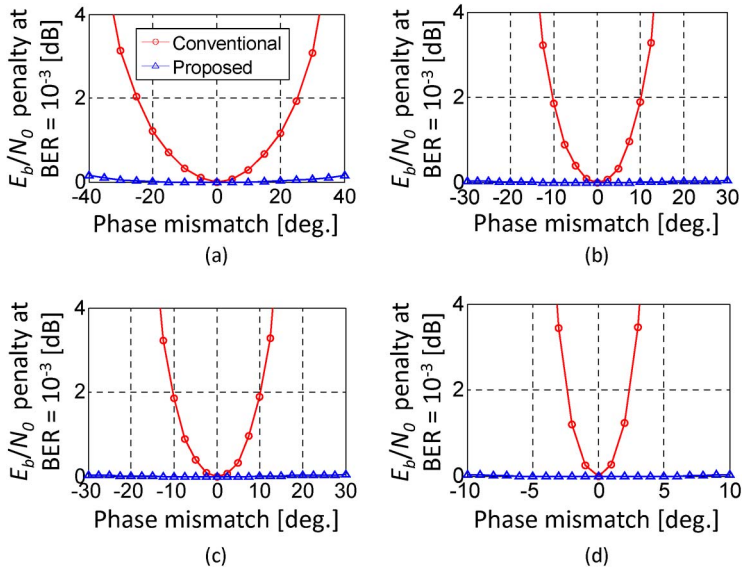

Fig. 3. E_b/N_0 penalty at BER of 10^{-3} as a function of the IQ phase mismatch when neither IQ gain mismatch nor IQ delay skew is included. (a) 4-QAM. (b) 16-QAM. (c) 64-QAM. (d) 256-QAM. Red and blue curves represent the penalty when the conventional configuration and the proposed configuration are used, respectively.

4. Simulation Results and Discussions

To validate the proposed scheme, we conduct simulations on 10-Gsymbol/s dual-polarization 4-, 16-, 64-, and 256-QAM coherent systems. In the transmitter, the signal is band limited by a root-raised-cosine filter with a roll-off factor of 0.5. The signal is then impaired by phase noise of the transmitter laser and passes through a 100-km-long standard single-mode fiber (SSMF), whose transfer function consists of a chromatic-dispersion value of 1700 ps/nm and a Jones matrix for fiber birefringence. Additive white Gaussian noise (AWGN) from a preamplifier and phase noise from LO are then given to the signal. The 3-dB linewidths of lasers for the transmitter and LO are 500 kHz, 100 kHz, 10 kHz, and 1 kHz for 4-, 16-, 64-, and 256-QAM systems, respectively. To obtain the optimal performance, the signal is subsequently filtered by another root-raised-cosine filter to match the signal waveform shaped at the transmitter. After that, we intentionally introduce IQ imbalances. Identical amounts of IQ imbalances are added to both of the *x*- and *y*-polarization ports. The signal is then sampled at twice the symbol rate and fed into the adaptive FIR filters configured as either in the conventional manner [see Fig. 2(a)] or in the proposed way [see Fig. 2(b)]. The delay-tap spacing is $T/2$, where T is the symbol duration. Such FIR filters simultaneously perform clock recovery, equalization of linear impairments, polarization demultiplexing, and IQ-imbalance compensation. The step-size parameter for the LMS algorithm is optimized so that bit-error rate (BER) is minimized. Next, carrier phase estimation based on the decision-directed LMS algorithm [18], symbol decoding, and BER calculations is done in this order. For the performance evaluation of different modulation formats, we calculate the penalty for the energy-per-bit-to-noise spectral-power-density ratio, i.e., E_b/N_0, at BER of 10^{-3}. In the following, results for the *x*-polarization tributary are presented; however, similar results are found for the *y*-polarization tributary.

Fig. 3 shows the E_b/N_0 penalty for different IQ phase mismatches when neither IQ gain mismatch nor IQ delay skew is included. In the simulation, we assume that $\delta_{x-I} = \delta_{y-I} = 0^\circ$ and vary the rotation angle of the Q axis $\delta_{x-Q} = \delta_{y-Q}$ to generate the IQ phase mismatch. In the conventional configuration, tolerances for the IQ phase mismatch are about 25°, 10°, 5°, and 2.5° for 4-, 16-, 64-, and 256-QAM formats, respectively, when the E_b/N_0 penalty is less than 2 dB. However, no notable penalty is found over a wide range when the proposed scheme is used.

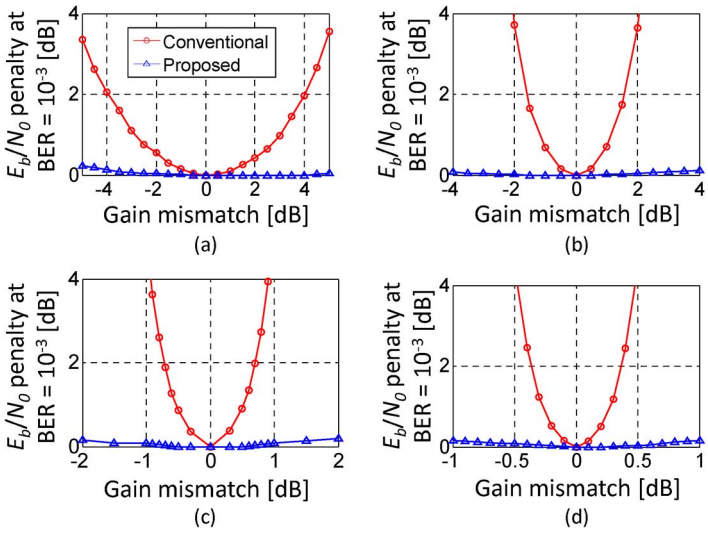

Fig. 4. E_b/N_0 penalty at BER of 10^{-3} as a function of the IQ gain mismatch when neither IQ phase mismatch nor IQ delay skew is included. (a) 4-QAM. (b) 16-QAM. (c) 64-QAM. (d) 256-QAM. Red and blue curves represent the penalty when the conventional configuration and the proposed configuration are used, respectively.

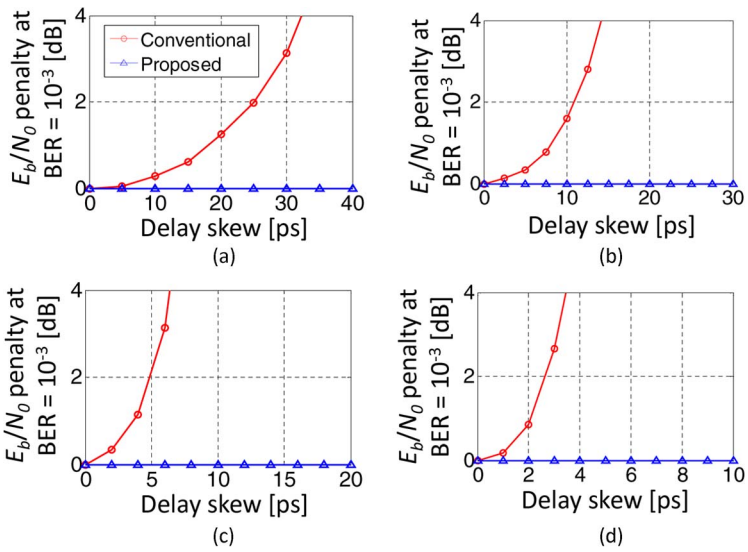

Fig. 5. E_b/N_0 penalty at BER of 10^{-3} as a function of the IQ delay skew when neither IQ phase nor IQ gain mismatch is included. (a) 4-QAM. (b) 16-QAM. (c) 64-QAM. (d) 256-QAM. Red and blue curves represent the penalty when the conventional configuration and the proposed configuration are used, respectively.

The E_b/N_0 penalty as a function of the IQ gain mismatch is shown in Fig. 4 when neither IQ phase mismatch nor IQ delay skew is included. We set the gain of the I port as a reference such that $\alpha_{x-I} = 1$ and $\alpha_{y-I} = 1$ and vary α_{x-Q} and α_{y-Q} to introduce the IQ gain mismatch. As far as the E_b/N_0 penalty is less than 2 dB, tolerances of the conventional configuration are about 4 dB, 1.75 dB, 0.75 dB, and 0.4 dB for 4-, 16-, 64-, and 256-QAM formats, respectively. However, with the proposed scheme, no significant penalty is observed over a wide range of the IQ gain mismatch.

Next, we calculate the E_b/N_0 penalty due to the IQ delay skew when neither IQ gain nor IQ phase mismatch is involved. As shown in Fig. 5, we find that the conventional FIR-filtering scheme is very

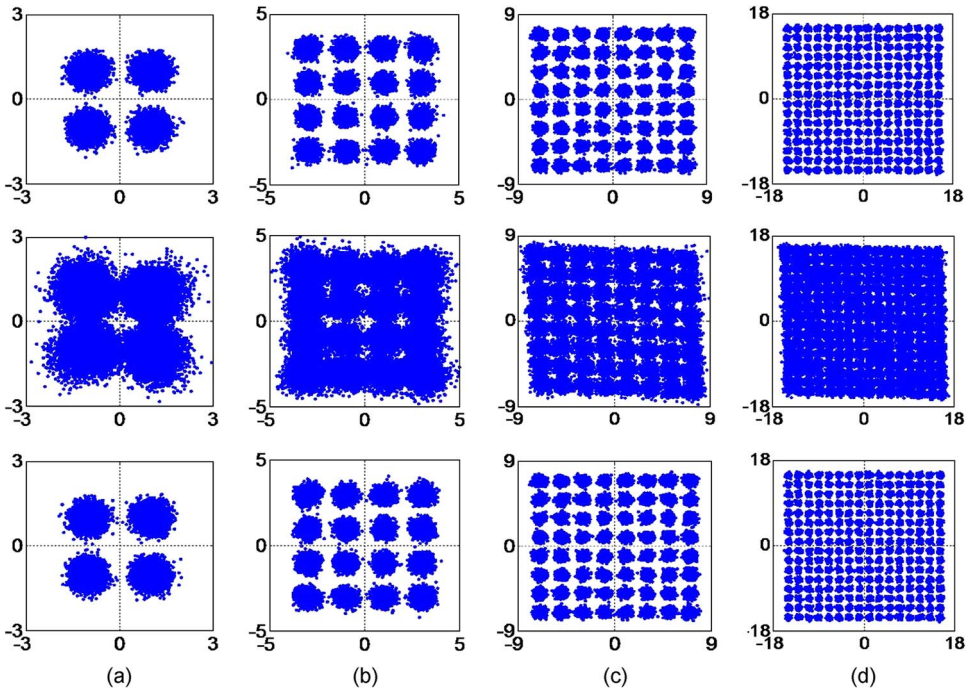

Fig. 6. Constellation diagrams of the recovered signal for (a) 4-QAM, (b) 16-QAM, (c) 64-QAM, and (d) 256-QAM formats. Upper diagrams show constellation maps when the conventional FIR-filter configuration is used and any IQ imbalance is not included. Middle diagrams are those with the conventional FIR-filter configuration when IQ imbalances given in Table 1 are involved. Lower diagrams are constellation maps calculated with the proposed scheme when the same IQ imbalances are included.

TABLE 1

Values of IQ imbalances used in che Calculation of constellation maps shown in Fig. 6

Modulation format	δ [deg.]	α [dB]	τ [ps]
4-QAM	20	-4	20
16-QAM	10	-2	10
64-QAM	6	-0.7	6
256-QAM	3	-0.4	4

sensitive to the IQ delay skew and the tolerance drastically decreases with the increase in the level of modulation; however, the proposed method has a very wide range of tolerance to such IQ delay skew. In fact, a quasi-continuous delay can be generated even by using $T/2$-spaced FIR filters, as shown in [14]. Therefore, any amount of delay skew can be compensated for with $T/2$-spaced FIR filters having a sufficient number of delay taps.

Finally, we investigate the combined effect of all of the IQ imbalances. Fig. 6 shows constellation diagrams for different modulation formats. In the simulation, E_b/N_0 for each polarization are 10 dB, 14 dB, 18 dB, and 23 dB for 4-, 16-, 64-, and 256-QAM formats, respectively. Upper diagrams show constellation maps calculated with the conventional FIR-filter configuration when any IQ imbalances are not included. Middle and lower diagrams are calculated with the conventional and proposed schemes, respectively, when IQ imbalances listed in Table 1 are included. As shown in the middle diagrams, the conventional approach fails to compensate for the IQ imbalances. However, the lower constellations are as clear as the upper constellations, showing that the proposed method can perfectly compensate for those IQ imbalances.

In our simulations, we do not include the effect of the limited ADC resolution. However, we generally need ADCs with higher bit resolution as the increase in the IQ imbalance. This situation is similar to other IQ-imbalance compensation methods.

It is also important to mention the computational complexity of the proposed scheme compared with that of the conventional FIR-filter scheme. The hardware-implementation complexity for a multiplier is much higher than that of an adder. Hence, if we evaluate the computational complexity in terms of the number of real multiplications, the conventional FIR-filter configuration and the proposed configuration have the same computational cost. This is because a complex-number multiplication in the DSP circuit is realized by using four real-number multiplications.

5. Conclusion

We have proposed a novel FIR-filter configuration, which can compensate for IQ imbalances generated in the front-end circuit of coherent optical receivers. With intensive computer simulations, we have evaluated the impact of IQ imbalances on the performance of dual-polarization 4-, 16-, 64-, and 256-QAM systems and verified that the proposed scheme can effectively compensate for them.

References

[1] E. Yamazaki, S. Yamanaka, Y. Kisaka, T. Nakagawa, K. Murata, E. Yoshida, T. Sakano, M. Tomizawa, Y. Miyamoto, S. Matsuoka, J. Matsui, A. Shibayama, J. Abe, Y. Nakamura, H. Noguchi, K. Fukuchi, H. Onaka, K. Fukumitsu, K. Komaki, O. Takeuchi, Y. Sakamoto, H. Nakashima, T. Mizuochi, K. Kubo, Y. Miyata, H. Nishimoto, S. Hirano, and K. Onohara, "Fast optical channel recovery in field demonstration of 100-Gbit/s Ethernet over OTN using real-time DSP," *Opt. Exp.*, vol. 19, no. 14, pp. 13 139–13 184, Jul. 2011.

[2] P. J. Winzer and R.-J. Essiambre, "Advanced optical modulation formats," in *Optical Fiber Telecommunication*, V. B. I. P. Kaminow, T. Li, and A. E. Willner, Eds. Amsterdam, The Netherlands: Elsevier, 2008.

[3] M. Seimetz, "Laser linewidth limitations for optical systems with high-order modulation employing feed forward digital carrier phase estimation," presented at the Opt. Fiber Commun. Conf., San Diego, CA, USA, Mar. 2008, Paper OTuM2.

[4] K. Kikuchi, "Analyses of wavelength- and polarization-division multiplexed transmission characteristics of optical quadrature-amplitude-modulation signals," *Opt. Exp.*, vol. 19, no. 19, pp. 17 985–17 995, Sep. 2011.

[5] Md. S. Faruk and K. Kikuchi, "Front-end IQ-error compensation in coherent optical receivers," presented at the Opto-Electron. Commun. Conf., Busan, Korea, Jul. 2012, Paper 4B2_5.

[6] K. Kikuchi, "Coherent optical communications: Historical perspectives and future directions," in *High Spectral Density Optical Communication Technology*, M. Nakazawa, K. Kikuchi, and T. Miyazaki, Eds. New York, NY, USA: Springer-Verlag, 2010.

[7] S. J. Savory, "Digital coherent optical receivers: Algorithms and subsystems," *IEEE J. Sel. Topics Quantum Electron.*, vol. 16, no. 5, pp. 1164–1179, Sep./Oct. 2010.

[8] T. Tanimura, S. Oda, T. Tanaka, T. Hoshida, Z. Tao, and J. C. Rasmussen, "A simple digital skew compensator for coherent receiver," presented at the Eur. Conf. Opt. Commun., Vienna, Austria, Sep. 2009, Paper 7.3.2.

[9] I. Fatadin, S. J. Savory, and D. Ives, "Compensation of quadrature imbalance in an optical QPSK coherent receiver," *IEEE Photon. Technol. Lett.*, vol. 20, no. 20, pp. 1733–1735, Oct. 2008.

[10] S. H. Chang, H. S. Chung, and K. Kim, "Impact of quadrature imbalance in optical coherent QPSK receiver," *IEEE Photon. Technol. Lett.*, vol. 21, no. 11, pp. 709–711, Jun. 2009.

[11] C. S. Petrou, A. Vgenis, I. Roudas, and L. Raptis, "Quadrature imbalance compensation for PDM QPSK coherent optical systems," *IEEE Photon. Technol. Lett.*, vol. 21, no. 24, pp. 1876–1878, Dec. 2009.

[12] S. Haykin, *Adaptive Filter Theory*, 4th ed. Englewood Cliffs, NJ, USA: Prentice-Hall, 2001.

[13] D. N. Godard, "Self-recovering equalization and carrier tracking in two-dimensional data communication systems," *IEEE Trans. Commun.*, vol. COM-28, no. 11, pp. 1867–1875, Nov. 1980.

[14] K. Kikuchi, "Clock recovering characteristics of adaptive finite-impulse-response filters in digital coherent optical receivers," *Opt. Exp.*, vol. 19, no. 6, pp. 5611–5619, Mar. 2011.

[15] K. Kikuchi, "Performance analyses of polarization demultiplexing based on constant-modulus algorithm in digital coherent optical receivers," *Opt. Exp.*, vol. 19, no. 10, pp. 9868–9880, May 2011.

[16] S. J. Savory, "Digital filters for coherent optical receivers," *Opt. Exp.*, vol. 16, no. 2, pp. 804–817, Jan. 2008.

[17] Md. S. Faruk, Y. Mori, C. Zhang, K. Igarashi, and K. Kikuchi, "Multi-impairment monitoring from adaptive finite-impulse-response filters in a digital coherent receiver," *Opt. Exp.*, vol. 18, no. 26, pp. 26 929–26 936, Dec. 2010.

[18] Y. Mori, C. Zhang, and K. Kikuchi, "Novel configuration of finite-impulse-response filters tolerant to carrier-phase fluctuations in digital coherent optical receivers for higher-order quadrature amplitude modulation signals," *Opt. Exp.*, vol. 20, no. 24, pp. 26 236–26 251, Nov. 2012.